

Decoupling Long- and Short-Term Patterns in Spatiotemporal Inference

Junfeng Hu
junfengh@u.nus.edu
School of Computing
National University of Singapore
Singapore

Yuxuan Liang
yuxliang@comp.nus.edu.sg
School of Computing
National University of Singapore
Singapore

Zhencheng Fan
zhencheng.fan@student.uts.edu.au
Faculty of Engineering and
Information Technology
University of Technology Sydney
Australia

Yifang Yin
yifang@comp.nus.edu.sg
School of Computing
National University of Singapore
Singapore

Ying Zhang
izhangying@nwpu.edu.cn
School of Computer Science
Northwestern Polytechnical
University
China

Roger Zimmermann
rogerz@comp.nus.edu.sg
School of Computing
National University of Singapore
Singapore

ABSTRACT

Sensors are the key to sensing the environment and imparting benefits to smart cities in many aspects, such as providing real-time air quality information throughout an urban area. However, a prerequisite is to obtain fine-grained knowledge of the environment. There is a limit to how many sensors can be installed in the physical world due to non-negligible expenses. In this paper, we propose to infer real-time information of any given location in a city based on historical and current observations from the available sensors (termed spatiotemporal inference). Our approach decouples the modeling of short-term and long-term patterns, relying on two major components. Firstly, unlike previous studies that separated the spatial and temporal relation learning, we introduce a joint spatiotemporal graph attention network that learns the short-term dependencies across both the spatial and temporal dimensions. Secondly, we propose an adaptive graph recurrent network with a time skip for capturing long-term patterns. The adaptive adjacency matrices are learned inductively first as the inputs of a recurrent network to learn dynamic dependencies. Experimental results on four public real-world datasets show that our method reduces state-of-the-art baseline mean absolute errors by 5% ~ 12%.

CCS CONCEPTS

• Information systems → Spatial-temporal systems; • Computing methodologies → Artificial intelligence.

KEYWORDS

Spatiotemporal inference, graph neural network

1 INTRODUCTION

In recent years, a large number of sensors have been deployed in different locations to sense the environment. They constantly report spatially-correlated and time-varying readings, such as traffic flows on roads and air quality measurements. Real-time monitoring of the spatiotemporal data is of great importance to smart city efforts. For example, real-time air quality information (e.g., concentration of PM2.5 particles) can support air pollution control and inform

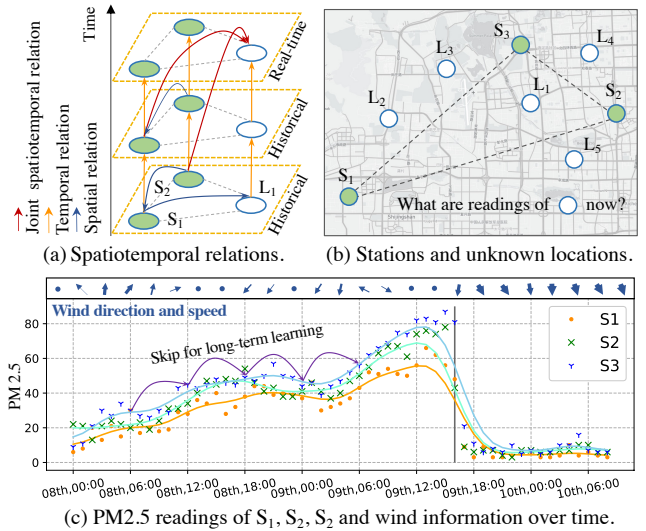


Figure 1: (a) Examples of three types of spatiotemporal relations. (b) Distribution of stations and unknown locations. (c) PM2.5 readings and wind condition. The curves represent approximated trends and arrows are time skips for long-term learning.

people’s decision making (e.g., whether to go out for cycling). However, a critical prerequisite for the above benefits is the fine-grained deployment of sensors, which may lead to considerable expense and high energy consumption [32]. In this paper, we study the problem of spatiotemporal inference: given historical and real-time readings of existing sensors, our target is to infer the real-time and fine-grained information *anywhere*. Fig. 1(b) shows an example, in which we leverage both historical and current readings of S_1 – S_3 to infer the real-time air quality status of locations L_1 – L_5 , without actual sensors in those places. The inference problem can be regarded as an upstream task of spatiotemporal data analysis like time series forecasting but remains less explored than the forecasting tasks which have made significant progress.

Spatiotemporal inference requires delicate spatial and temporal dependencies modeling. For spatial relations, the most prevalent traditional methods might be k -nearest neighbors or inverse distance weighting. They borrow spatial information from surrounding sensors to infer unknown locations. However, the complex relations are often restricted to be linear, therefore not reflecting real data characteristics. Recently, deep learning methods have been the dominant model for spatiotemporal inference. Among them, Graph Neural Networks (GNNs) are widely used by virtue of their ability to handle non-Euclidean sensory data in graph structures [4, 9, 27]. For instance, [1] learns to deduce the reading of a location according to neighbors' information. Meanwhile, temporal dependencies are also significant to the task. A simple strategy is to concatenate input frames along the channel dimension and obtain interpolations of all time points at once so that temporal relations are extracted among channels [24]. For spatiotemporal topics like time series forecasting, more prevalent approaches rely on combining GNNs with recurrent neural networks (RNNs) [10] or temporal convolutional networks (TCNs) [25] to learn spatial and temporal dynamics separately. While having proven to be effective for capturing relations, these approaches encounter two major shortcomings.

First, current studies for spatiotemporal inference ignore the different long- versus short-term patterns in the time series data. For example, reading points are fluctuating within a short period in Fig. 1(c). However, when focusing on the smoothed curves from 00:00 to the next day at 12:00, they still follow an increasing trend. This is evidence that the long- and short-term relations have inconsistent influences. A GNN based inference method [24] regards temporal dependencies uniformly, which ignores this inconsistency. A natural approach is to adopt an RNN, as the recurrent structure pays more attention to recent frames. However, the gradient vanishing problem makes it hard to capture either long-term trends or fine-grained short-term patterns.

Second, existing models are still far from effectively learning complex and dynamic spatiotemporal relationships. As Fig. 1(a) is illustrating, a location is affected by both spatial relations in the graph (i.e., blue arrows) and its historical readings in the temporal dimension (i.e., orange arrows). Moreover, there exist more complicated *joint spatiotemporal dependencies* (i.e., red arrows) in which a location is influenced by sensors at different locations and times directly. Unfortunately, the above GNN-RNN modeling structures fail to explicitly capture them, which limits the model's ability. The recent attention methods like [8, 31] also separate the spatial and temporal learning into two attention blocks followed by the feature aggregation. Further, relations are even hidden and highly dynamic. In Figs. 1(b) and (c), S_2 is geographically close to S_3 but around 16:00 of 09/11/2017, the PM2.5 concentration of S_2 is close to that of S_1 . One plausible reason might be the dynamic change of the wind conditions.

To tackle these issues, we propose a Long- Short-term Joint Spatio-Temporal Network (LSJSTN) for real-time sensory spatiotemporal inference based on graph structures. LSJSTN decouples short- and long-term learning into two components: a Joint SpatioTemporal Graph Attention neTwork (JST-GAT) and an Adaptive Skip Graph Gated Recurrent Unit (ASG-GRU). The first component adopts attention blocks to compute the impact between a node and other

nodes in different neighbor frames. Subsequently, GNN is utilized to aggregate information from all nodes at all neighbor frames with the attention maps. In this way, JST-GAT learns joint spatiotemporal relations explicitly, discarding the separate learning structures. On the other hand, impacts are measured using sensor dynamic readings, which further improve its ability of modeling hidden and dynamic relations. For the second component, we first propose an inductive version of adaptive adjacency matrix learning to enhance the ability of capturing long-term dynamic relations, given that the existing methods [25, 26] are transductive which cannot handle the dynamic input graph structure. Then, we introduce a GRU unit with a time skip that maintains a temporal span but with fewer steps, which enables the model to focus on the long-term temporal trends. Note that our model is also designed and trained inductively which deals with a variable number of input sensors using a graph sampling strategy without retraining the model [30].

We compare our model with state-of-the-art baselines on real-world datasets. Results demonstrate that our model surpasses them with an obvious margin. We further visualize the attention weights interpreting the ability of our LSJSTN at modeling dynamic spatiotemporal relations. Our main contributions are summarized in four-fold as follows:

- We propose a new learning based framework for spatiotemporal inference, which decouples the long- and short-term patterns learning into separate modules.
- For effective spatiotemporal modeling for fine-grained short-term dependencies, we introduce a JST-GAT module that measures the impact weights between nodes in different time and spatial dimension simultaneously, which captures the joint spatiotemporal relations explicitly.
- We propose a ASG-GRU, in which the skip operation maintains the temporal span with fewer recurrent steps to facilitate the long-term patterns modeling. Meanwhile, the adaptive adjacency matrix learning module is improved for handling dynamic input graph structure of various input sensors in the inductive environment.
- Our LSJSTN model achieves the state-of-the-art performances over four benchmark datasets in diverse applications including METR-LA, PsMS-Bay, NREL, and BJ-Air, which demonstrates the effectiveness and generalization ability of our proposed method.

2 PRELIMINARIES

2.1 Problem Formulation

A graph is represented by $\mathcal{G} = (\mathcal{V}, \mathcal{E}, \mathbf{A})$, where \mathcal{V} is the node set ($|\mathcal{V}| = N$), \mathcal{E} is the set of edges, and $\mathbf{A} \in \mathbb{R}^{N \times N}$ is the pre-defined adjacency matrix. At time t , we have readings $\mathbf{X}_t = [\mathbf{x}_t^1, \dots, \mathbf{x}_t^N] \in \mathbb{R}^{N \times D}$, where D is the number of attributes of a node. Following the inductive setting, at each training epoch, we randomly sample a subgraph and its corresponding readings \mathbf{X}_t^s . Then, the readings are further divided into *known sensors* $\mathbf{X}_t^s \in \mathbb{R}^{N_k \times D}$ and *unknown locations* $\mathbf{Y}_t^s \in \mathbb{R}^{N_u \times D}$.

At each time t , the task of real-time spatiotemporal inference uses historical and real-time known sensors $\{\mathbf{X}^s\}_{:,t}$ with its subgraph structure \mathcal{G}^s to infer signals of unknown locations at time t by the

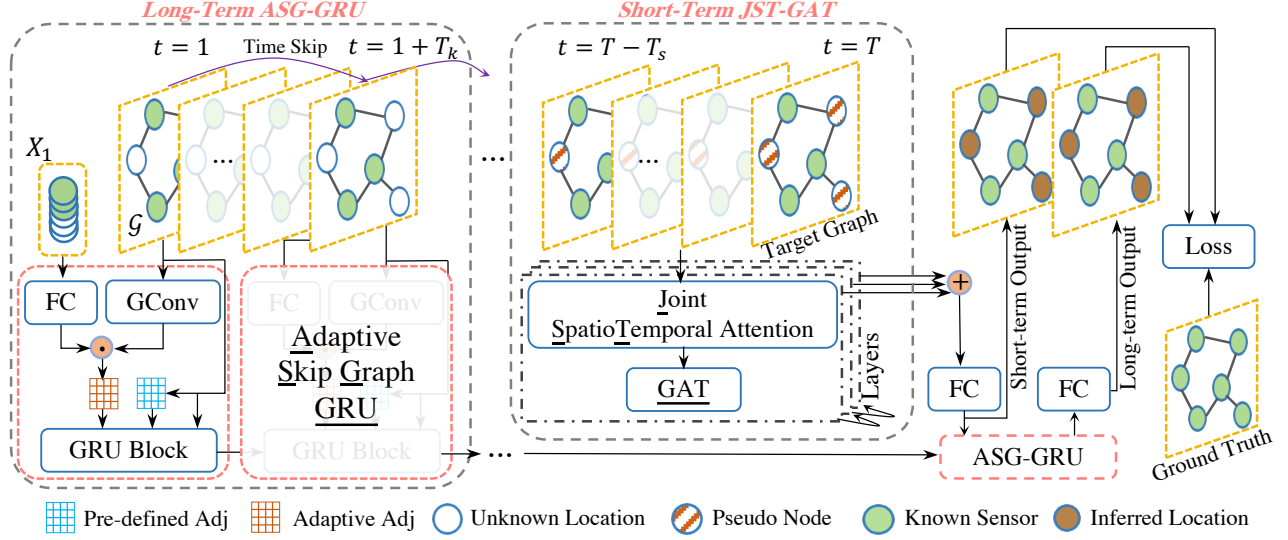


Figure 2: The framework of the proposed LSJSTN model. Adj: adjacency matrix.

following equation:

$$\{X^s\}_{:t}; \mathcal{G}^s \xrightarrow{f(\cdot)} [\hat{Y}_t^s], \quad (1)$$

where $\hat{Y}_t^s \in \mathbb{R}^{N_u \times D}$ refers to inferred unknown locations in the target graph and $f(\cdot)$ is the learned mapping function. The superscript s will be dropped in the remaining paper for brevity. To simplify the problem, at time t , we only use historical and current readings of time window T . Note that the model is trained with certain sensors but applicable to any location by adjusting the adjacency matrix during inference.

2.2 Graph Convolution

As an essential operation to learn interactions among nodes based on the graph structure [12], the graph convolutional layer can be defined as:

$$Z = \phi\left(\sum_{l=1}^L \tilde{A}^l X W^l\right), \quad (2)$$

where $\tilde{A} = D^{-1}A \in \mathbb{R}^{N \times N}$ denotes the normalized adjacency matrix with self-loops, D is the degree matrix, $X \in \mathbb{R}^{N \times D}$ are the input readings, $W^l \in \mathbb{R}^{D \times F}$ are learnable parameters, $\phi(\cdot)$ is the activation function, and L is the order of graph convolution. To capture hidden relationships between two nodes that a pre-defined adjacency matrix cannot reflect, [26] propose a graph convolution with adaptive adjacency matrix, which results in:

$$Z = \phi\left(\sum_{l=1}^L \tilde{A}^l X W_p^l + \hat{A}^l X W_d^l\right), \quad (3)$$

where \hat{A} is the adaptive adjacency matrix learned by the network. We term these two convolutions as $\Theta_{\star \mathcal{G}}(X, \tilde{A})$ and $\Theta_{\star \mathcal{G}}(X, \tilde{A}, \hat{A})$, where Θ are learnable parameters.

3 METHODOLOGY

Fig. 2 shows the overall framework of our LSJSTN model. It consists of two components for long- and short-term spatiotemporal patterns learning. The short-term JST-GAT first generates *pseudo nodes* for unknown locations. Then, several spatiotemporal attention and graph convolution layers are used to learn joint spatiotemporal dependencies, and obtain short-term inference results. The long-term ASG-GRU learns an adaptive adjacency matrix in an inductive approach each time after certain skips. Then, the graph GRU utilizes the adaptive adjacency matrices as inputs to encode historical sensor readings and integrates short-term inferences to generate long-term results in the last step.

3.1 Joint Spatiotemporal Graph Attention Network

3.1.1 k -nearest Inverse Distance Weighting. As we do not have readings of unknown locations in a graph, the attention mechanism is not applicable. Thus, we first introduce a k -nearest inverse distance weighting (k -IDW) for short-term unknown locations (i.e., *pseudo nodes*), given the target graph and its short-term neighbor frames of window T_s . As shown in the yellow arrows of Fig. 3, it follows the idea of k -nearest neighbor that first searches the spatially k -nearest known sensors for each unknown location. Then, the inverse distances of the location to its neighbors are adopted as weights to calculate the weighted mean:

$$\hat{y}_{pn} = \frac{\sum_{i=1}^k x^i \odot d^{i-\rho}}{\sum_{i=1}^k d^{i-\rho}}, \quad (4)$$

where k denotes the assigned number of nearest neighbors, d^i is the distance between a location to the neighbor x^i , ρ is the decay rate, and \odot represents the Hadamard product. Then, we can regard *pseudo nodes* and known sensors uniformly notated as $X_t = [x_t^1, \dots, x_t^{N_k}, \hat{y}_{pn}^1, \dots, \hat{y}_{pn}^{N_u}] \in \mathbb{R}^{N \times D}$.

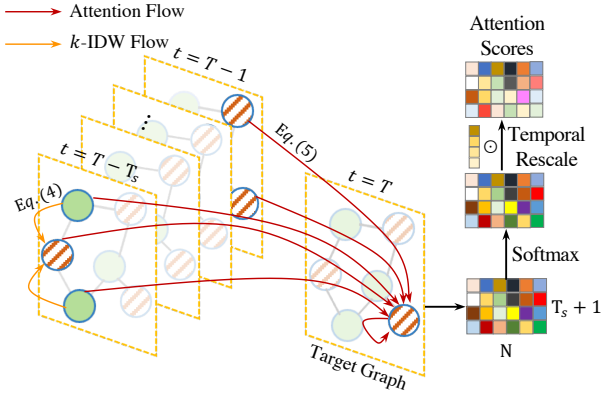


Figure 3: Illustrations and information flows of k -nearest inverse distance weighting and the joint spatiotemporal attention. Only a limited number of flows for one node are drawn.

3.1.2 Joint Spatiotemporal Attention. Sensor readings are influenced by measurements from other sensors in the spatiotemporal vicinity. However, the influences might be highly dynamic and difficult to capture. To this end, previous works [8, 15] utilize separate attention modules to handle the dynamic relations in spatial and temporal dimensions, respectively. However, these models fail to explicitly consider joint spatiotemporal dependencies. For instance, assuming wind from the north, PM2.5 matter will be blown toward the south over time. Meanwhile, a car accident will cause a traffic jam on an upstream road later. Inspired by such complex interactions, we propose a novel joint spatiotemporal attention mechanism to capture dynamic joint spatiotemporal relations, illustrated in Fig. 3.

Given a neighbor frame \mathbf{X}_t in window T_s and the target frame \mathbf{X}_T , we first calculate attention weights for the sensor x_T^i to every x_t^j formulated by:

$$e_t^{i,j} = \mathbf{v}_a^\top \tanh(\mathbf{W}_a \mathbf{x}_T^i + \mathbf{U}_a \mathbf{x}_t^j + \mathbf{b}_a), \quad (5)$$

$$e_t^{i,j} = \frac{\exp(e_t^{i,j})}{\sum_{j=1}^N \exp(e_t^{i,j})}, \quad (6)$$

where $\mathbf{v}_a, \mathbf{b}_a \in \mathbb{R}^F$, $\mathbf{W}_a, \mathbf{U}_a \in \mathbb{R}^{D \times F}$ are learnable parameters. Note that the parameters are shared across all frames to reduce the number of parameters. The attention weights measure the information strength between two nodes, which represents the joint spatiotemporal correlations. We also compute attention scores within the target graph so that only the spatial relations are captured. In the end, we obtain attention maps $[\mathbf{E}_{T-T_s}, \dots, \mathbf{E}_T] \in \mathbb{R}^{(T_s+1) \times N \times N}$, where the first dimension N refers to sensors of current time T and the second N means historical sensors. Based on the assumption that near frames have higher temporal influences, we further rescale the attention maps by:

$$\mathbf{E} = [e^{-T_s \lambda} \mathbf{E}_{T-T_s}, \dots, e^{-\lambda} \mathbf{E}_{T-1}, e^{-0 \lambda} \mathbf{E}_T], \quad (7)$$

where λ is used to control the weight decay rate.

3.1.3 Joint Spatiotemporal Graph Convolution. After rescaling the attention maps, we feed sensor signals of the short-term frames, the pre-defined adjacency matrix as well as the attention maps into the joint spatiotemporal graph convolution module to learn short-term inference representations:

$$\begin{aligned} \mathbf{Z}_t^l &= \gamma \mathbf{X}_t + \mu \mathbf{E}_t \odot \tilde{\mathbf{A}} \mathbf{Z}_t^{l-1}, \\ \mathbf{Z}^{out} &= \sum_{t=T-T_s}^T \phi \left(\sum_{l=1}^L \mathbf{Z}_t^l \mathbf{W}_s^l + \mathbf{b}_s^l \right), \end{aligned} \quad (8)$$

where γ, μ are hyperparameters for residual connection \mathbf{X}_t and learned features, $\mathbf{Z}_t^l \in \mathbb{R}^{N \times D}$ are feature states at time t , where $\mathbf{Z}_t^0 = \mathbf{X}_t$, $\mathbf{Z}^{out} \in \mathbb{R}^{N \times F}$ are output features. In case of the directed graph that contains bi-directional adjacency matrices, we utilize two attention and convolution modules denoted as \rightarrow and \leftarrow , and transform the Eq. 8 into:

$$\begin{aligned} \mathbf{Z}_t^l &= \gamma \mathbf{X}_t + \mu \mathbf{E}_t \mathbf{A} \mathbf{Z}_t^{l-1}, \\ \mathbf{Z}_t^l &= \gamma \mathbf{X}_t + \mu \mathbf{E}_t \mathbf{A} \mathbf{H}_t^{l-1}, \\ \mathbf{Z}^{out} &= \sum_{t=T-T_s}^T \phi \left(\sum_{l=1}^L \mathbf{Z}_t^l \mathbf{W}_s + \mathbf{Z}_t^l \mathbf{W}_s + \mathbf{b}_s^l \right). \end{aligned} \quad (9)$$

Then, we adopt a fully connected layer to get the short-term inference outputs:

$$\hat{\mathbf{Y}}_T^s = \mathbf{Z}^{out} \mathbf{W}_{f_s} + \mathbf{b}_{f_s}, \quad (10)$$

where $\mathbf{W}_{f_s} \in \mathbb{R}^{F \times D}$, $\mathbf{b}_{f_s} \in \mathbb{R}^D$ are parameters and $\hat{\mathbf{Y}}_T^s \in \mathbb{R}^{N \times D}$ are short-term inferences. Note that the attention and graph convolution can be stacked in several layers. Finally, the joint spatiotemporal dependencies can be learned by single JST-AGN. Further, the attention block aids in the interpretation by visualizing weights to understand how the model learns the dynamic spatiotemporal relations.

3.2 Adaptive Skip Graph Gated Recurrent Unit

3.2.1 Inductive Adaptive Graph Generation. To model the hidden relations among nodes, [3, 25, 26] learn a static adaptive adjacency matrix but disregard the dynamic dependencies. Later, [13] handles the dynamic relations by learning the matrix at each recurrent step. However, these methods significantly depend on the node embedding layer which is not available in the inductive settings. Thus, we propose an inductive adaptive graph generation module that updates the adjacency matrix in an inductive fashion. To be specific, at time step t , we use the historical hidden states \mathbf{H}_{t-T_k} , \mathbf{X}_t and $\tilde{\mathbf{A}}$ to learn graph-level information. Here, the T_k is the skip that will be described below. Then, we replace the node embedding layer with a fully connected layer $FC(\cdot)$ to capture node-level features. The adaptive adjacency matrix $\hat{\mathbf{A}}_t$ at time t can be calculated by:

$$\begin{aligned} \mathbf{M}_t^1 &= \tanh(\Theta_{1 \star \mathcal{G}}(\mathbf{X}_t | \mathbf{H}_{t-T_k}, \tilde{\mathbf{A}})) \odot FC(\mathbf{X}_t), \\ \mathbf{M}_t^2 &= \tanh(\Theta_{2 \star \mathcal{G}}(\mathbf{X}_t | \mathbf{H}_{t-T_k}, \tilde{\mathbf{A}})) \odot FC(\mathbf{X}_t), \\ \hat{\mathbf{A}}_t &= \text{ReLU}(\tanh(\alpha(\mathbf{M}_t^1 \mathbf{M}_t^{2 \top} - \mathbf{M}_t^2 \mathbf{M}_t^{1 \top}))), \end{aligned} \quad (11)$$

along the channel dimension where $|$ is the channel-wise concatenation, \mathbf{M}_t^1 and $\mathbf{M}_t^2 \in \mathbb{R}^{N \times F}$ are source node encoding and target

node encoding, respectively, $\sigma(\cdot)$ is the sigmoid activation function and α is the saturation rate hyperparameter. In the directed graph situation, graph convolutions of two directions are employed which we do not describe here for brevity.

3.2.2 Skip Graph Gated Recurrent Unit. GRU [5] is one of the recurrent structures designed to memorize the historical temporal information. However, the gradient vanishing and overwhelming state estimation of recent time step inputs cause difficulties for the model to capture long-term temporal patterns [2]. To alleviate this issue, we propose a graph GRU with skip to maintain a temporal relations span but with fewer recurrent steps. To be specific, current hidden states are updated using historical hidden states of a certain number of skips T_k , which can be formulated as:

$$\begin{aligned} \mathbf{r}_t &= \sigma(\Theta_{r\star} \mathcal{G}(\mathbf{X}_t | \mathbf{H}_{t-T_k}, \tilde{\mathbf{A}}, \hat{\mathbf{A}}) + \mathbf{b}_r), \\ \mathbf{u}_t &= \sigma(\Theta_{u\star} \mathcal{G}(\mathbf{X}_t | \mathbf{H}_{t-T_k}, \tilde{\mathbf{A}}, \hat{\mathbf{A}}) + \mathbf{b}_u), \\ \mathbf{c}_t &= \tanh(\Theta_{c\star} \mathcal{G}(\mathbf{X}_t | (\mathbf{H}_{t-T_k} \odot \mathbf{r}_t), \tilde{\mathbf{A}}, \hat{\mathbf{A}}) + \mathbf{b}_c), \\ \mathbf{H}_t &= \mathbf{u}_t \odot \mathbf{H}_{t-T_k} + (1 - \mathbf{u}_t) \odot \mathbf{c}_t, \end{aligned} \quad (12)$$

where \mathbf{r}_t and $\mathbf{u}_t \in \mathbb{R}^{N \times F}$ are a reset gate and update gate, respectively. Through the recurrent skip, the module is encouraged to focus on the long-term temporal patterns, which ignores low-level relations among consecutive frames and the limited recurrent steps also facilitate the optimization process. At the last recurrent step at which the short-term inference results are available, we feed the $\hat{\mathbf{Y}}_T^s$ to the graph GRU to compute the hidden states \mathbf{H}_T and obtain the long-term outputs after a fully connected layer:

$$\hat{\mathbf{Y}}_T^l = \mathbf{H}_T \mathbf{W}_{fl} + \mathbf{b}_{fl}, \quad (13)$$

where $\mathbf{W}_{fl} \in \mathbb{R}^{F \times D}$, $\mathbf{b}_{fl} \in \mathbb{R}^D$ are parameters, and $\hat{\mathbf{Y}}_T^l \in \mathbb{R}^{N \times D}$ are long-term inference outputs.

To facilitate the generalization ability of the model, we train the model by reconstructing all sensor readings at time T instead of just unknown locations like [1] and simultaneously optimize the L_2 loss of short-term outputs $\hat{\mathbf{Y}}_T^s$ and long-term results $\hat{\mathbf{Y}}_T^l$.

4 EXPERIMENTS

4.1 Experimental Settings

4.1.1 Datasets. We evaluate the performances of LSJSTN on four real-world spatiotemporal datasets in diverse application scenarios: 1) **METR-LA**: traffic speed dataset collected from 207 sensors in the highway of Los Angeles, 2) **PeMS-Bay**: a traffic speed dataset collected by California Transportation Agencies containing 325 sensors in the Bay Area, 3) **NREL**: solar power dataset recorded by 137 photovoltaic power stations in Alabama state, 4) **BJ-Air**: air quality index dataset from 35 air quality stations in Beijing and here, we consider the PM2.5 observations. We construct the pre-defined adjacency matrix $\hat{\mathbf{A}}$ based on either road network distance or geospatial distance. Then the Gaussian kernel method [22] formulated as $\tilde{\mathbf{A}}_{i,j} = \exp(-\frac{\text{dist}(v_i, v_j)^2}{\sigma^2})$ is applied, where σ is the standard deviation, $\text{dist}(v_i, v_j)$ means the distance between sensor v_i and v_j . The statistics of datasets are listed at Table 1.

4.1.2 Baseline Methods. We compare the performances of our model with five baselines as follows:

Dataset	METR-LA	PeMS-Bay	NREL	BJ-Air
Category	Traffic Spd	Traffic Spd	Solar Energy	Air Quality
Adjacency Matrix	rn-dis	rn-dis	geo-dis	geo-dis
# Sensors	207	325	137	35
# Time points	34,272	52,116	105,120	10,228
Frequency	5-min	5-min	5-min	1-hour
Mean	58.45	62.62	15.96	60.99
Standard Deviation	13.08	9.58	9.86	65.31

Table 1: Dataset statistics. #: the number. Traffic Spd: traffic speed. Rn-dis/Geo-dis: road-network/geospatial distance.

- **KNN**: K-nearest neighbors interpolates readings of unknown locations by averaging the K nearest sensors in the spatial dimension.
- **IDW**: Inverse distance weighting is based on distances between nodes and calculates the weighted average of available nodes as interpolations of each unknown location [17].
- **OKriging**: Ordinary kriging is a classic statistical interpolation method based on the geospatial locations of the sensors and a Gaussian process [6].
- **KCN**: Kriging convolutional network first builds a graph using k -nearest neighbors for an unknown location, and then adopts a graph neural network to interpolate the location independently in the spatial dimension [1].
- **IGNNK**: Inductive Graph Neural Network Kriging, which is one of the latest state-of-the-art models for spatiotemporal interpolation that can be trained in an inductive approach [24].

Among these baselines, KNN, IDW and OKriging are statistical methods, while KNN and IGNNK are deep learning models.

4.1.3 Evaluation Metrics. We adopt three criteria to evaluate our model: the root mean square error (RMSE), the mean absolute error (MAE), and the R-Square (R^2). All of them are frequently used in regression problems.

Algorithm 1 Training Procedure of LSJSTN

Require: graph $\mathcal{G} = (\mathcal{V}, \mathcal{E}, \mathbf{A})$; sensor readings of training set $\{\mathbf{X}\}$; time window T ; initialized model LSJSTN().

Ensure: optimized learnable weights.

- 1: **for** $i = 1 \rightarrow \text{Num_Iteration}$ **do**
 - 2: Initialize batch list $\mathcal{X} = [], \mathcal{Y} = []$.
 - 3: {Sampling Graph}
 - 4: $\mathcal{G}^s, \{\mathbf{X}^s\}, \{\mathbf{Y}^s\} = \text{Graph Sampling}(\mathcal{G}, \{\mathbf{X}\})$.
 - 5: **for** $j = 1 \rightarrow \text{Batch_Size}$ **do**
 - 6: Randomly choose a start time t .
 - 7: Append $\{\mathbf{X}^s\}_{t:t+T}$ to \mathcal{X} .
 - 8: Append $\{\mathbf{Y}^s\}_{t:t+T}$ to \mathcal{Y} .
 - 9: **end for**
 - 10: $\hat{\mathbf{Y}}^{short}, \hat{\mathbf{Y}}^{long} = \text{LSJSTN}(\mathcal{G}^s, \mathcal{X}, \mathcal{Y})$.
 - 11: Compute $L_2(\hat{\mathbf{Y}}^{short}, \mathcal{Y}) + L_2(\hat{\mathbf{Y}}^{long}, \mathcal{Y})$ and derive the gradients.
 - 12: Update learnable weights using the optimizer.
-

Model	METR-LA			PeMS-Bay			NREL			BJ-Air			#Params
	MAE	RMSE	R^2	MAE	RMSE	R^2	MAE	RMSE	R^2	MAE	RMSE	R^2	
KNN	7.65 \pm 0.00	11.20 \pm 0.00	0.30	6.45 \pm 0.00	12.16 \pm 0.00	-0.62	3.28 \pm 0.00	4.62 \pm 0.00	0.78	18.35 \pm 0.00	29.41 \pm 0.00	0.78	-
IDW	7.78 \pm 0.00	11.53 \pm 0.00	0.26	6.38 \pm 0.00	11.78 \pm 0.00	-0.52	3.08 \pm 0.00	4.46 \pm 0.00	0.79	17.80 \pm 0.00	28.21 \pm 0.00	0.81	-
OKriging	-	-	-	-	-	-	2.81 \pm 0.00	4.23 \pm 0.00	0.80	17.98 \pm 0.00	28.62 \pm 0.00	0.81	-
KCN	7.24 \pm 0.05	10.76 \pm 0.07	0.35	5.11 \pm 0.06	8.31 \pm 0.07	0.24	2.41 \pm 0.09	3.88 \pm 0.08	0.84	15.63 \pm 0.23	26.36 \pm 0.33	0.83	18K
IGNNK	7.08 \pm 0.09	10.56 \pm 0.04	0.37	4.12 \pm 0.08	7.15 \pm 0.08	0.44	2.30 \pm 0.06	3.54 \pm 0.08	0.87	14.52 \pm 0.22	25.85 \pm 0.29	0.84	45K
LSJSTN	6.75\pm0.09	10.01\pm0.06	0.44	3.92\pm0.06	6.80\pm0.07	0.49	2.03\pm0.08	3.11\pm0.07	0.90	13.34\pm0.21	24.36\pm0.31	0.85	16K

Table 2: Performance comparison and number of learnable parameters for different methods on four datasets. K: thousand.

4.1.4 Implementation Details. Our LSJSTN and the deep-learning baselines are implemented with PyTorch 1.7 and trained on an NVIDIA Quadro RTX 6000 GPU. For the hyperparameters, we set decay rates ρ and λ to 1, saturation rate α to 2, and impact factors γ , μ to 0.1 and 0.9. The time sequence length T is 25 in which the time window for short-term learning is $T_s = 3$. The skipping number of GRU T_k equals 4, i.e., we feed readings of sensors into the network every 4 steps each time. The activation function ϕ is ReLU. The number of layers for JSAGN is 3 and the size of hidden states for graph GRU is 16. All the learnable parameters are initialized with the Xavier normalization [7]. The model is trained by minimizing the L2 loss function under the Adam [11] optimizer and the learning rate of 10^{-3} . Note that we keep the same settings for all datasets, which verifies the good generalization ability of our model. For the dataset division, we use the first 70% of the time points to train models and validate or test models using the following 20% and 10%, respectively. For sensor division, we manually leave 50% of the sensors out for testing, called testing sensors, and the remaining 50% as training sensors. At each epoch, we randomly mask 50% of the training sensors as unknown locations. When evaluating models, we use all training sensors to interpolate all testing sensors. To ensure a fair comparison, we use the same division of training and testing sensors and run each deep learning model five times independently to report the average results and the standard deviations. Algorithm. 1 summarizes the training procedure of LSJSTN.

4.2 Model Comparison

Table 2 reports the overall performance of our LSJSTN and other baselines on four datasets. We can clearly see that our approach consistently outperforms all the baselines over all metrics, which shows the superiority of our LSJSTN. To be specific, the LSJSTN reduces the errors by (4.6%, 4.9%, 11.7%, 8.1%) and (5.2%, 4.9%, 12.1%, 5.8%) compared to the state-of-the-art IGNNK on MAE and RMSE, respectively. Meanwhile, the deep learning models surpass the performance of statistical methods, which provides evidence that deep models successfully learn spatiotemporal dependencies. Then, both IGNNK and our model outperform the results of KCN, because it only focuses on the spatial modeling, ignoring the temporal relations. Among four datasets, we find the R^2 metrics on METR-LA and PsMS-Bay are smaller than for the remaining datasets because of their smaller standard deviations when referring to their mean values. We also notice that on the Beijing-Air dataset, the results of the three deep learning models have larger deviations, which means that the training process is not stable. We conjecture that

this is due to the limited number of sensors and the large standard deviation of readings so that models have difficulty to learning general spatiotemporal dependencies. LSJSTN has fewer parameters than other models, which also shows its learning ability.

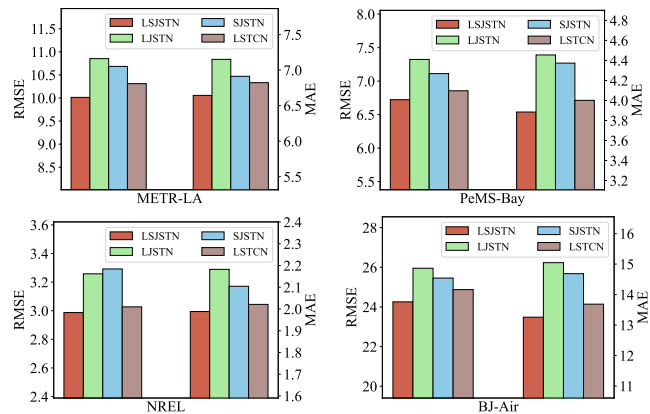


Figure 4: Parameters study among different variants.

4.3 Ablation Study

After model comparison, we investigate the effectiveness of each module in LSJSTN.

4.3.1 Effects of long- and short-term learning. We explore two variants: 1) **LJSSTN**: a long-term learning model that only contains the adaptive skip graph gated recurrent unit, 2) **SJSTN**: a short-term learning model that adopts just a joint spatiotemporal attention graph network which takes short-term frames as the inputs. As illustrated in Fig. 4, compared to LSJSTN, both LJSSTN and SJSTN obtain obviously poor results. Comparing these variants, we find SJSTN performs better. These observations demonstrate that 1) decoupling long- and short-term learning improves performance, and 2) sensor readings have much larger relevance to the short-term patterns but follow the trend of long-term patterns.

4.3.2 Effects of joint spatiotemporal attention. We replace the joint attention module of our model with the temporal convolution network (TCN) which follows the same structures as [26] and keep the number of parameters similar. From Fig. 4, we observe that LSJSTN has relatively better performance compared to LSTCN. We argue that this is because the joint attention module explicitly takes

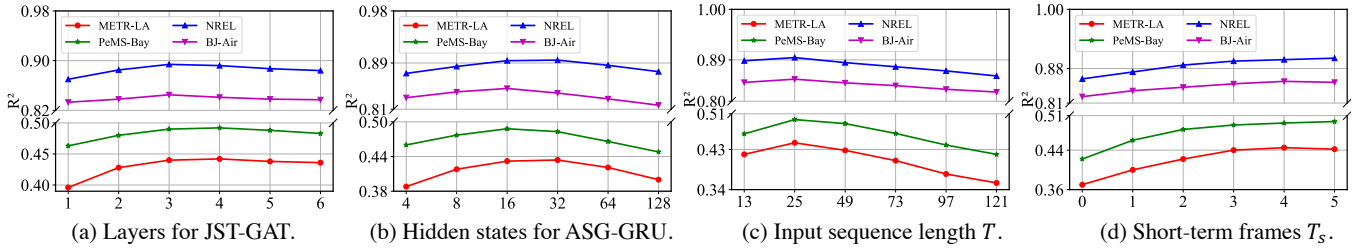


Figure 5: Parameters study among different variants on four datasets.

joint spatiotemporal relations into consideration, which reduces the challenge of modeling complex relations.

4.4 Hyperparameter Study

We further study the performance of our LSJSTN under different parameter settings and report the results of R^2 . In each experiment, we modify the settings of just one parameter and keep others unchanged as the default settings.

4.4.1 Effects of number of layers of JST-AGN. We adjust the number of layers in the joint attention graph module and show the results in Fig. 5(a). The performance first increases and peaks at 3 or 4 layers. Then, R^2 remains stable or starts to decrease slightly. So, we uniformly keep the number of layers at 3 to reduce the computational cost.

4.4.2 Effects of size of hidden states of ASG-GRU. We change the size of the graph GRU’s hidden states from 4 to 128. As shown in Fig. 5(b), we find that the results increase until the size of 16 or 32 and then start to decrease, indicating that the model starts to overfit. Accordingly, we set the size to 16.

4.4.3 Effects of time sequence length T . We keep the skip step $T_k = 4$ and adjust the input time sequence length T to evaluate the ability of GRU to model long-term patterns. As expected, in Fig. 5(c), a longer input sequence cannot guarantee better results. This is because of the gradient vanishing problem of GRU on long-term modeling and in this situation, the long historical features start to resemble *noise* that hampers the model’s performance.

4.4.4 Effects of number of short-term frames T_s . Finally, we modify the number of short-term frames T_s . As illustrated in Fig. 5(d), as T_s increases, we observe that the performance first increases fast and then levels off. The main reason is that a longer successive sequence will provide more information about the spatiotemporal dependencies but less information density. In this case, a fine-grained learning module like JSTAGN is suboptimal to model long-term patterns. To this end, we set T_s to 3 and adopt a graph GRU for learning these patterns.

4.5 Case Study

The attention block in our model provides interpretability by indicating which sensors are more related. To further investigate the ability of our LSJSTN on modeling dynamic relationships, we conduct a case study using the BJ-Air dataset from 0:00 to 12:00 on 03/09/2017 and visualize the attention weights of the target

graph. For succinctness, we equally sample 13 out of 35 sensors as shown in Fig. 6(a) and use the center station S21 to discuss. Fig. 6(b) shows the results of 12 consecutive hours where stations are drawn according to their relative orientations to S21. Given the southeastern condition of the time period, we observe the following. 1) Stations S8, S13, and S17 have larger weights, which means that these stations contribute more to the inference of S21. 2) Geographical information contained in the predefined adjacency matrix could reflect the spatial relations, as closer stations have a large influence (e.g., S29 and S31 to S21). 3) Static distances cannot guarantee genuine spatiotemporal dependencies. For instance, S13 is excessively far away from S21 compared to S18 but has an even larger impact. In this situation, the dynamic relations become dominant. These observations verify that our model captures both static spatial relations and dynamic implicit dependencies simultaneously even without knowing possible external factors.

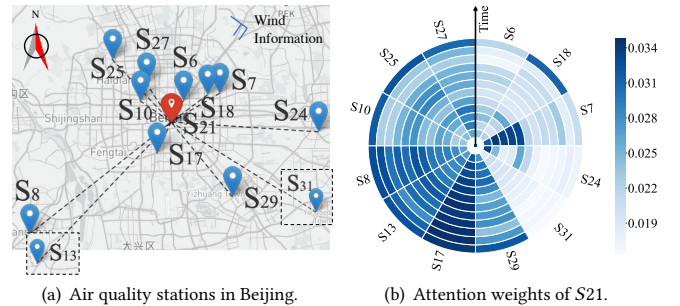


Figure 6: (a) Locations of air quality stations, where only the discussed sensors are shown. S21 is the target sensor to compute attention weights. Note that stations S13, S31 are extremely far from S21. (b) Attention scores of station S21.

5 RELATED WORK

5.1 Spatiotemporal Inference

In addition to k -nearest neighbors and inverse distance weighting, another traditional method for spatiotemporal inference is using a Gaussian Process. It adopts a kernel structure to estimate the variogram of spatial relations and then linearly interpolates unknown locations [6, 20]. However, the assumption of a Gaussian distribution is not always true and in that case, delicate transformation of non-Gaussian data is required [21]. Besides spatial modeling, [29] also considers temporal relations and fill missing readings with hybrid statistical variables from local-global spatiotemporal views.

Unfortunately, this method cannot handle the case when sensors are completely missing in the inference settings. Recently, deep learning methods have been widely introduced for inference. [1] describes a kriging convolutional network for spatial inference. The model finds k nearest neighbors for an unknown location and then extracts dependencies from neighboring sensors to infer readings of the locations using GCNs. However, this model discards temporal relations and only infers a single unknown location each time. Then, [24] focuses on spatiotemporal inference but concatenate time series data along the channel dimension as the GCNs' inputs, which regards temporal dependencies uniformly, ignoring the temporal relations inconsistency.

5.2 Spatiotemporal Graph Neural Network

With recent advances in deep learning, spatiotemporal graph neural networks have been the dominant class for spatiotemporal data modeling, following mainly two paradigms. They either couple GNNs with RNNs [18, 19] or TCNs [16, 23, 25, 28]. In the first category, GNNs are employed as basic building blocks for capturing spatial dependencies while RNNs are used to model temporal dynamics. For example, a pioneering study [14] first proposes a diffusion convolution that learns the spatial relations through bidirectional random walks on the graph, and then integrates it into RNNs for temporal modeling. In the second category, TCNs are adopted to learn temporal relationships and enjoy faster running speed than RNNs. For instance, [25] proposes a dilated inception temporal convolution to discover relations with different scales and enlarge receptive fields of the model for long sequence modeling. To address hidden relations among sensors, [3, 13] further propose graph generation modules that learn an adaptive adjacency matrix to describe the hidden relation strength between two nodes. However, these models are based on transductive learning, which cannot handle a variable number of input nodes and are less explored for inference problems. Meanwhile, they have overlooked the joint spatiotemporal dependencies.

6 CONCLUSIONS AND FUTURE WORKS

In this study, we propose a novel LSJSTN model for real-time spatiotemporal inference. To better learn the short- and long-term patterns, we decouple the model into two components: a joint spatiotemporal graph attention network and an adaptive skip graph gated recurrent unit. Extensive experiments on four real-world applications demonstrate that our LSJSTN consistently outperforms previous state-of-the-art methods by 5%~12% on MAE. Moreover, we visualize the attention weights to show the interpretation of our approach, revealing its capability to learn both static and dynamic relations. In the future, we will integrate external factors (e.g., wind conditions, POI) into the model to capture external dynamics explicitly. Meanwhile, the idea of joint spatiotemporal attention can be transferred to time series forecasting for better capturing spatiotemporal relations.

REFERENCES

[1] Gabriel Appleby, Linfeng Liu, and Li-Ping Liu. 2020. Kriging Convolutional Networks. In *Proceedings of the AAAI Conference on Artificial Intelligence*, Vol. 34. 3187–3194.

[2] Dzmitry Bahdanau, Kyunghyun Cho, and Yoshua Bengio. 2015. Neural Machine Translation by Jointly Learning to Align and Translate. In *3rd International Conference on Learning Representations, ICLR*.

[3] Lei Bai, Lina Yao, Can Li, Xianzhi Wang, and Can Wang. 2020. Adaptive Graph Convolutional Recurrent Network for Traffic Forecasting. In *Advances in Neural Information Processing Systems 33: Annual Conference on Neural Information Processing Systems, NeurIPS*.

[4] Joan Bruna, Wojciech Zaremba, Arthur Szlam, and Yann LeCun. 2014. Spectral Networks and Locally Connected Networks on Graphs. In *2nd International Conference on Learning Representations, ICLR, Banff, AB, Canada, April 14-16, 2014, Conference Track Proceedings*.

[5] Junyoung Chung, Caglar Gulcehre, KyungHyun Cho, and Yoshua Bengio. 2014. Empirical evaluation of gated recurrent neural networks on sequence modeling. *arXiv preprint arXiv:1412.3555* (2014).

[6] Noel Cressie. 2015. *Statistics for spatial data*. John Wiley & Sons.

[7] Xavier Glorot and Yoshua Bengio. 2010. Understanding the difficulty of training deep feedforward neural networks. In *Proceedings of the thirteenth international conference on artificial intelligence and statistics*. JMLR Workshop and Conference Proceedings, 249–256.

[8] Shengnan Guo, Youfang Lin, Ning Feng, Chao Song, and Huaiyu Wan. 2019. Attention based spatial-temporal graph convolutional networks for traffic flow forecasting. In *Proceedings of the AAAI Conference on Artificial Intelligence*, Vol. 33. 922–929.

[9] William L Hamilton, Rex Ying, and Jure Leskovec. 2017. Inductive representation learning on large graphs. In *Proceedings of the 31st International Conference on Neural Information Processing Systems*. 1025–1035.

[10] Jindong Han, Hao Liu, Hengshu Zhu, Hui Xiong, and Dejing Dou. 2021. Joint Air Quality and Weather Prediction Based on Multi-Adversarial Spatiotemporal Networks. In *Proceedings of the 35th AAAI Conference on Artificial Intelligence*.

[11] Diederik P. Kingma and Jimmy Ba. 2015. Adam: A Method for Stochastic Optimization. In *3rd International Conference on Learning Representations, ICLR, Yoshua Bengio and Yann LeCun (Eds.)*.

[12] Thomas N Kipf and Max Welling. 2016. Semi-supervised classification with graph convolutional networks. *arXiv preprint arXiv:1609.02907* (2016).

[13] Fuxian Li, Jie Feng, Huan Yan, Guangyin Jin, Depeng Jin, and Yong Li. 2021. Dynamic Graph Convolutional Recurrent Network for Traffic Prediction: Benchmark and Solution. *arXiv preprint arXiv:2104.14917* (2021).

[14] Yaguang Li, Rose Yu, Cyrus Shahabi, and Yan Liu. 2018. Diffusion Convolutional Recurrent Neural Network: Data-Driven Traffic Forecasting. In *6th International Conference on Learning Representations, ICLR*.

[15] Yuxuan Liang, Songyu Ke, Junbo Zhang, Xiwen Yi, and Yu Zheng. 2018. GeoMAN: Multi-level Attention Networks for Geo-sensory Time Series Prediction. In *Proceedings of the Twenty-Seventh International Joint Conference on Artificial Intelligence, IJCAI* 3428–3434.

[16] Yuxuan Liang, Kun Ouyang, Junkai Sun, Yiwei Wang, Junbo Zhang, Yu Zheng, David Rosenblum, and Roger Zimmermann. 2021. Fine-Grained Urban Flow Prediction. In *Proceedings of the Web Conference 2021*. 1833–1845.

[17] George Y Lu and David W Wong. 2008. An adaptive inverse-distance weighting spatial interpolation technique. *Computers & geosciences* 34, 9 (2008), 1044–1055.

[18] Zheyi Pan, Yuxuan Liang, Weifeng Wang, Yong Yu, Yu Zheng, and Junbo Zhang. 2019. Urban traffic prediction from spatio-temporal data using deep meta learning. In *Proceedings of the 25th ACM SIGKDD International Conference on Knowledge Discovery & Data Mining*. 1720–1730.

[19] Zheyi Pan, Wentao Zhang, Yuxuan Liang, Weinan Zhang, Yong Yu, Junbo Zhang, and Yu Zheng. 2020. Spatio-temporal meta learning for urban traffic prediction. *IEEE Transactions on Knowledge and Data Engineering* (2020).

[20] Carl Edward Rasmussen. 2003. *Gaussian processes in machine learning*. In *Summer school on machine learning*. Springer.

[21] Hirotsuka Saito and Pierre Goovaerts. 2000. Geostatistical interpolation of positively skewed and censored data in a dioxin-contaminated site. *Environmental Science & Technology* 34, 19 (2000), 4228–4235.

[22] David I Shuman, Sunil K Narang, Pascal Frossard, Antonio Ortega, and Pierre Vandergheynst. 2013. The emerging field of signal processing on graphs: Extending high-dimensional data analysis to networks and other irregular domains. *IEEE signal processing magazine* 30, 3 (2013), 83–98.

[23] Junkai Sun, Junbo Zhang, Qiaofei Li, Xiwen Yi, Yuxuan Liang, and Yu Zheng. 2020. Predicting citywide crowd flows in irregular regions using multi-view graph convolutional networks. *IEEE Transactions on Knowledge and Data Engineering* (2020).

[24] Yuankai Wu, Dingyi Zhuang, Aurélie Labbe, and Lijun Sun. 2021. Inductive Graph Neural Networks for Spatiotemporal Kriging. In *Proceedings of the 35th AAAI Conference on Artificial Intelligence*. 4478–4485.

[25] Zonghan Wu, Shirui Pan, Guodong Long, Jing Jiang, Xiaojun Chang, and Chengqi Zhang. 2020. Connecting the dots: Multivariate time series forecasting with graph neural networks. In *Proceedings of the 26th ACM SIGKDD International Conference on Knowledge Discovery & Data Mining*. 753–763.

[26] Zonghan Wu, Shirui Pan, Guodong Long, Jing Jiang, and Chengqi Zhang. 2019. Graph WaveNet for Deep Spatial-Temporal Graph Modeling. In *Proceedings of*

- the Twenty-Eighth International Joint Conference on Artificial Intelligence, IJCAI*. 1907–1913.
- [27] Keyulu Xu, Weihua Hu, Jure Leskovec, and Stefanie Jegelka. 2019. How Powerful are Graph Neural Networks?. In *7th International Conference on Learning Representations, ICLR, New Orleans, LA, USA, May 6-9, 2019*.
- [28] Sijie Yan, Yuanjun Xiong, and Dahua Lin. 2018. Spatial temporal graph convolutional networks for skeleton-based action recognition. In *Thirty-second AAAI conference on artificial intelligence*.
- [29] Xiuwen Yi, Yu Zheng, Junbo Zhang, and Tianrui Li. 2016. ST-MVL: Filling Missing Values in Geo-Sensory Time Series Data. In *Proceedings of the Twenty-Fifth International Joint Conference on Artificial Intelligence, IJCAI*. 2704–2710.
- [30] Hanqing Zeng, Hongkuan Zhou, Ajitesh Srivastava, Rajgopal Kannan, and Viktor K. Prasanna. 2020. GraphSAINT: Graph Sampling Based Inductive Learning Method. In *8th International Conference on Learning Representations, ICLR*.
- [31] Chuanpan Zheng, Xiaoliang Fan, Cheng Wang, and Jianzhong Qi. 2020. Gman: A graph multi-attention network for traffic prediction. In *Proceedings of the AAAI Conference on Artificial Intelligence*.
- [32] Yu Zheng, Furu Liu, and Hsun-Ping Hsieh. 2013. U-air: When urban air quality inference meets big data. In *Proceedings of the 19th ACM SIGKDD international conference on Knowledge discovery and data mining*. 1436–1444.